PERGAMON

International Journal of Solids and Structures 37 (2000) 919–942

INTERNATIONAL JOURNAL OF SOLIDS and STRUCTURES

www.elsevier.com/locate/ijsolstr

Modelling of the mechanical behavior and damage processes of fibrous ceramic matrix composites: application to a 2-D SiC/SiC

Gérald Camus*

Laboratoire des Composites Thermostructuraux, UMR 5801 (CNRS–SEP–UB1), Domaine Universitaire, 3 Allée de La Boëtie, 33600 Pessac, France

Received 23 June 1998; in revised form 26 February 1999

Abstract

A continuum damage mechanics constitutive model is developed to describe the mechanical behavior of fiber-reinforced ceramic matrix composites submitted to complex multiaxial loadings. This model relies on the use of a phenomenological internal damage variable defined as the change of the compliance tensor induced by any given loading. Microstructural observations of the damage entities provide qualitative data allowing us to formulate physically founded simplifying hypotheses. The evolution laws of scalar damage variables derived from the components of the compliance tensor are established within a classical thermodynamic framework, using coupled multicriteria expressed in the space of the associated thermodynamic forces. Damage deactivation processes related to the unilateral crack closure effect observed under compressive loadings are introduced through the definition of effective compliance tensor components. This approach is applied to a 2-D woven SiC/SiC composite processed by chemical vapor infiltration (CVI). Major advantages and drawbacks of the proposed approach as observed from various validation tests are discussed.

Keywords: Ceramic matrix composites; 2-D SiC/SiC; Continuum damage mechanics; Anisotropic damage; Constitutive model

1. Introduction

Fiber reinforced ceramic matrix composites (CMC) display an extended non-linear mechanical behavior related to the onset and growth of matrix microcracks and various associated fiber/matrix interactions such as debonding and sliding (Evans and Marshall, 1989). The progressive development of these various energy dissipating phenomena, collectively termed as damage, is highly anisotropic in

* Fax: +0033-5-56-84-12-25.
E-mail address: admin@lcts.u-bordeaux.fr (G. Camus)

0020-7683/00/$ - see front matter
PII: S0020-7683(99)00065-7

nature and is accompanied by an anisotropic degradation of the elastic properties of the composite leading to its final rupture. These damage mechanisms also present a markedly unilateral character, depending on whether matrix microcracks are closed or open, i.e. the material behaves differently under tensile and compressive loadings (Chaboche et al., 1995).

Damage mechanics, which relates the development of damage mechanisms inside a material to their effects on the elastic coefficients, may be considered as the modelling of these phenomena on a structural analysis scale. Since the early works of Kachanov (1958), damage mechanics has proved to be an efficient tool in predicting the constitutive behavior of a structure submitted to complex loadings for a wide variety of materials such as metals and concrete (Krajcinovic, 1989; Lemaître, 1992), and more recently fiber reinforced composites (including CMCs) (Ladevèze, 1994; Chaboche et al., 1995; Burr et al., 1997). The essentials of the damage mechanics approach to the formulation of constitutive laws for damaged materials may be classified into two large categories:

(i) The micromechanical approaches, aimed at establishing a functional dependence between the microdefects (as defined by geometrical parameters), the properties of the constituent materials and the macroscopic behavior. Properties of the continuous equivalent damaged medium are usually obtained through an homogenization method, either numerical or analytical (Duvaut, 1976; Laws and Dvorak, 1987; Gudmundson and Ostlund, 1992).
(ii) The meso and/or macroscopic approaches, which consist of measuring the effects of the internal morphological changes on the mechanical response through the introduction of an internal state variable, referred to as the damage variable, in the sense of irreversible thermodynamics (Harris et al., 1989; Talreja, 1991; Chaboche, 1993; Ladevèze, 1994). These approaches have given rise to a branch of continuum mechanics known as continuum damage mechanics (CDM).

Despite their advantages in taking into account physical reality with a minimum of ambiguity, the micromechanical approaches are usually unsuitable for modelling the general behavior of a real material (i.e. submitted to a multiaxial stress state) in which geometry and kinetic laws of the microdefects present a complex feature. Similar drawbacks may be underlined, yet to a lesser extend, with CDM approaches based on internal variables derived from microstructural damage entities (Harris et al., 1989; Talreja, 1991; Aussedat et al., 1993). Indeed, at least for CMCs and as far as structural computation is concerned, the most reliable behavioral models have been established with CDM approaches based on phenomenological internal variables directly derived from the mechanical response (Cluzel et al., 1992; Ladevèze et al., 1994; Chaboche et al., 1995; Aubard, 1995). Incidentally, it is worth mentionning that among these approaches, recent works have made the connection with the mechanisms revealed by research in materials science (Burr et al., 1995, 1997).

The goal of the present work is to establish a constitutive model of the mechanical behavior of CMCs submitted to complex multiaxial loadings, in view of being incorporated in appropriate finite-element codes allowing the effective design of complex components. The approach adopted in the present paper lies within the CDM framework and is restricted to materials possessing an orthotropic fibrous reinforcement. It uses a phenomenological internal damage variable based on a different definition than those encountered so far for CMCs. Following Ortiz, who first introduced this formulation in the case of concrete (Ortiz, 1985), the state of damage of the material is defined by the change of the compliance tensor induced by any given loading. In addition, microscopic observations of the onset and growth of the damage entities provide necessary guidelines for the formulation of physically founded simplifying hypotheses from which are derived the constitutive equations. The principal reproach usually made to the phenomenological CDM approaches, i.e. the lack of a well defined physical meaning of the damage variable, is thus partly overcome. Damage kinetics, i.e. the damage increase laws as a function of the imposed loading, are established within a classical thermodynamic framework, based on the introduction of two potentials, the thermodynamic potential and the dissipation potential (Bataille and

Kestin, 1979; Germain et al., 1983). Such a framework thus ensures thermodynamic consistency of the behavioral model, which is a regular prerequisite to an implementation into finite-elements codes.

This general approach is applied to a 2-D woven SiC/SiC composite processed via the chemical vapor infiltration (CVI) of a SiC matrix into a SiC–Nicalon fibrous preform. In order to obtain a clearer understanding of the basic hypotheses introduced in the development of the constitutive model, results and analysis of the mechanical behavior of the material are underlined first. Based on these results, the modelling approach and the inferred constitutive equations are then established. Finally, the various functions and parameters entering the model are identified and some experimental validations illustrating its applicability are given.

2. Material and experimental results

2.1. Material description

The 2-D SiC/SiC composite supporting the present model was processed by SEP (Société Européenne de Propulsion) by chemical vapor infiltration of SiC into a bidirectional fibrous preform consisting of a stack of SiC–Nicalon fiber woven fabrics (plain weave). Before infiltration by the matrix, the fibers received a proprietary surface treatment and were then coated with a pyrocarbon interphase in order to enhance the desired non-linear/non-catastrophic tensile behavior while preserving the stress to rupture (Jouin et al., 1993).

These processing steps resulted in flat rectangular plates of a material referred to as 2-D SiC/SiC 0.4% (i.e. with a mean failure strain of at least 0.4%) having a fiber content of approximately 35 vol.% and a residual porosity inherent to the CVI process in the range 10–15 vol.%. A comprehensive description of the microstructure of the material, which is beyond the scope of this paper, may be found in reference (Guillaumat, 1994).

It is worth mentioning that this 2-D SiC/SiC 0.4% is not fully identical to a commercially available material. Direct comparisons between present data and others should therefore be avoided as these materials may behave differently due to different processing conditions.

2.2. Mechanical behavior

The basic stress–strain curves summarizing the room temperature mechanical behavior of the material are displayed from Figs. 1–3. Results of the tests performed in tension, within the fiber axis and off-axis (at 20° and 45°), as well as in shear with the Iosipescu configuration, are taken from a previous study completed by Aubard (1992). In order to take into account the compressive behavior in the modelling approach, these former results were complemented by additional compression and tension/compression tests. Specimen design, test procedure and strain measurement methods have been thoroughly described previously (Aubard, 1992). It is yet important of note that all the tests were performed at a constant slow strain rate of 0.04% min^{-1}, insuring quasi-static loading conditions.

The tensile behavior proves to be quasi damageable-elastic, i.e. the material's apparent modulus progressively decreases as non-linearity takes place whereas residual strains observed upon complete unloading as well as loading/unloading hysteresis loops are weakly extended. Beyond an applied stress of about 150 MPa and up to final rupture, this behavior also presents an increasingly anisotropic character.

The compressive behavior is linear-elastic and brittle whatever the loading angle and, besides, remains unaffected by a preliminary damaging tensile loading: complete closure of the matrix microcracks generated in tension recovers the apparent initial modulus of the material. Furthermore, the

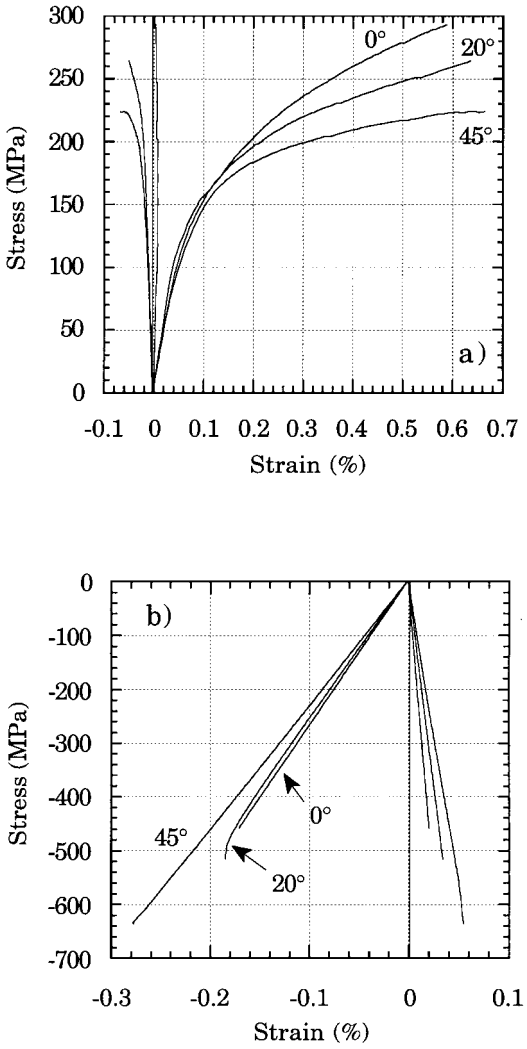

Fig. 1. Mechanical behavior of the 2-D SiC/SiC 0.4% in monotonic tension (a) and monotonic compression (b) for various loading angles.

prolongation of the unloading sequences in the compression domain does not appear to subsequently modify the tensile behavior when compared to similar monotonic tensile tests.

The dependence of the applied stress as a function of the in-plane transverse strain observed from a tensile test performed within the fiber axis evidences an important variation of the off-diagonal component of the compliance tensor, S_{12}. This term regularly increases once damage takes place, leading thus to a reversal in the transverse strain, up to a zero or even slightly positive value. Such a behavior may be related to the extension of debonding accompanying matrix microcracking: the progressive release of stresses in the matrix at and near the cracks surfaces increasingly reduces its lateral Poisson's contraction (Wang and Parvizi-Majidi, 1992). However, it should be emphasized that the magnitude of these transverse strains remains very small, i.e. less than 0.01% in absolute value. As in the case of the axial modulus, unloadings prolonged in the compression domain restitute the initial value S_{12}^0.

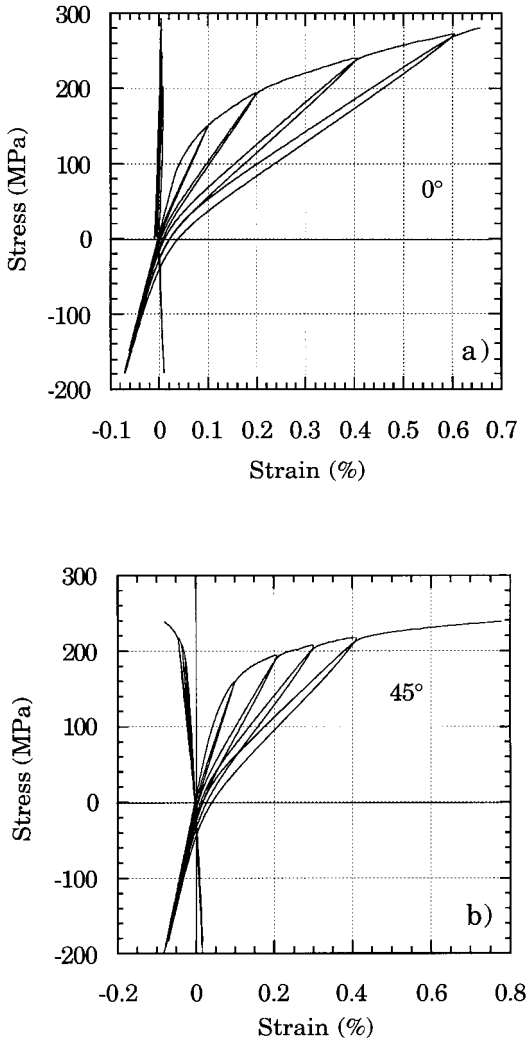

Fig. 2. Stress/strain curves for tension/compression loadings, (a) within the fiber axis, (b) at 45° off-axis.

The in-plane shear behavior may also be considered, with a good approximation, as damageable-elastic. It is characterized by a limited strain hardening, close to that displayed by the stress–strain response of the 45° off-axis tensile test, and an important angular strain to rupture.

Figs. 4 and 5 display typical microstructural changes taking place in the material when tested in tension under various loading angles. These microstructural characterizations were obtained through optical microscopy observations performed on polished samples cut from specimens tested to failure. They complement previous observations made in situ during the tests as well as on specimens taken from tests interrupted at different load levels (Aubard, 1992; Guillaumat, 1994).

Matrix microcracks generated under on-axis tension are predominantly orientated perpendicular to the applied load. Their development may be described on the basis of three major stages. A first cracking pattern initiates at the sharp singularities of macropores present in the inter-bundle matrix-rich region. A second family of cracks, referred to as longitudinal cracks, then takes place in the transverse

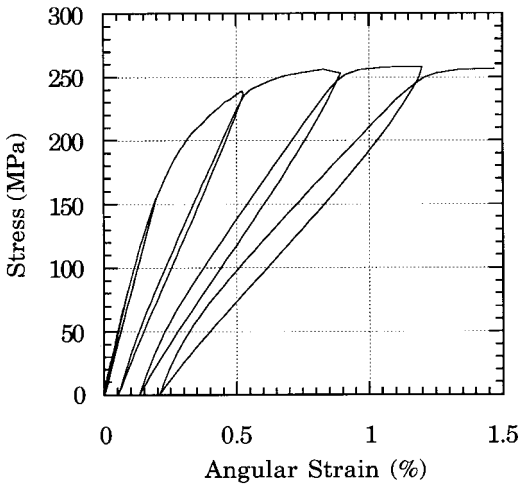

Fig. 3. Stress/strain response of the 2-D SiC/SiC 0.4% under in-plane Iosipescu shear.

bundles. The last stage involves the propagation of these two first generations of cracks in the longitudinal bundles followed by a subsequent intense additional matrix microcracking within these bundles (referred to as transverse cracks with a final crack spacing of about 15 μm).

The onset of the Iosipescu shear-induced damage also follows a multi-stage scheme but microcracks are, as previously attested by other authors (Cady et al., 1995), mainly inclined at about 45° to the fiber axes.

Microstructural characterization of the specimens tested under off-axis tension reveals that the first family of inter-bundle matrix microcracks is mainly inclined at 45° to the fiber axes, whereas both longitudinal, transverse and 45° microcracks may be observed inside the fiber bundles. It is also worth mentioning that, under 20° off-axis tension, few cracks tend to be tilted perpendicular to the loading axis.

3. Description of the proposed model

3.1. Definition of the damage variables

3.1.1. Basic hypotheses

The model is established under the general hypothesis of small isothermal displacements and quasi-static loadings (i.e. the damage phenomena are assumed to be time independent) for an average plane-stress state within the plane of the plies.

As originally proposed by Ortiz (1985), the state of damage of the material is directly characterized by the change of the compliance tensor induced by the imposed loading. This compliance tensor may thus be written under the following additive form:

$$\mathbf{S} = \mathbf{S}^0 + \Delta\mathbf{S} \tag{1}$$

in terms of the initial compliance tensor of the undamaged material $\mathbf{S}^0$ and the added compliance $\Delta\mathbf{S}$ linked to the presence of damage in the material. This fourth rank symmetrical tensor, $\Delta\mathbf{S}$, is thus defined as the internal variable representing the current state of damage in the material (Baste and

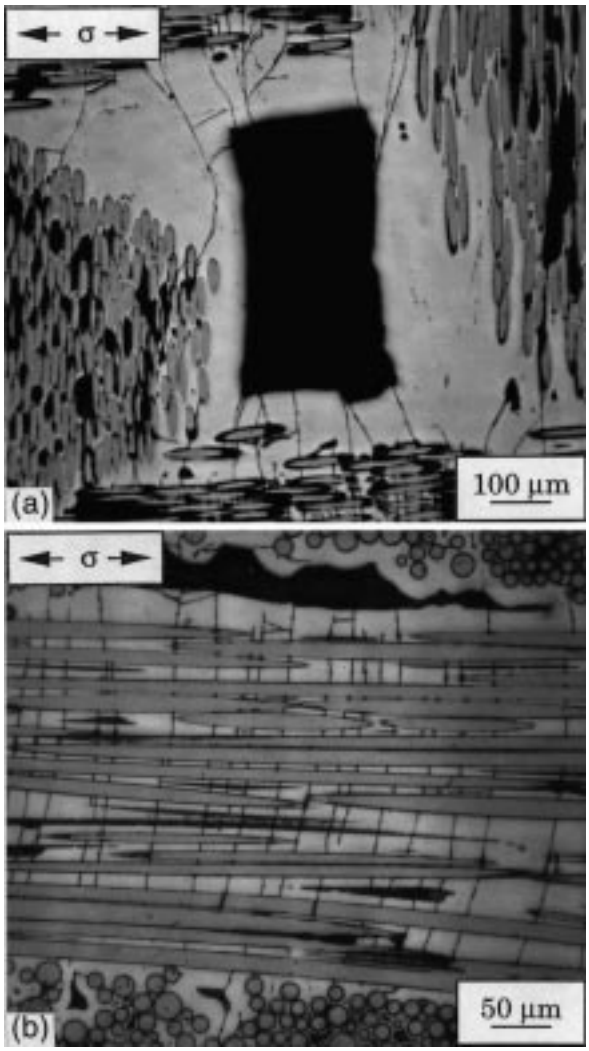

Fig. 4. Optical micrographs taken on a specimen tested to rupture in tension within the fiber axis showing: (a) inter-bundle matrix microcracks (plane (1,2)), (b) intra-bundle matrix microcracks (plane (1,3)).

Audouin, 1991). Such a definition allows for the description of induced anisotropic elastic degradation with a minimum of ambiguity while limiting the data base requirements to a minimum.

On the basis of the experimental results previously described, it may then be further assumed that:

(i) the fiber directions naturally represent the local orthotropy axes of the composite and this orthotropic symmetry is maintained throughout the damage processes,
(ii) the composite behaves as a damageable-elastic material, i.e. linear elasticity is assumed to hold if the damage state does not change.

The first assumption is supported by the microstructural analysis of the damage modes which has evidenced three main sets of microcracks with preferred orientation either normal, parallel and/or at 45° to the fiber bundles when a shear component is present. This last class of 45° cracks will thus be treated

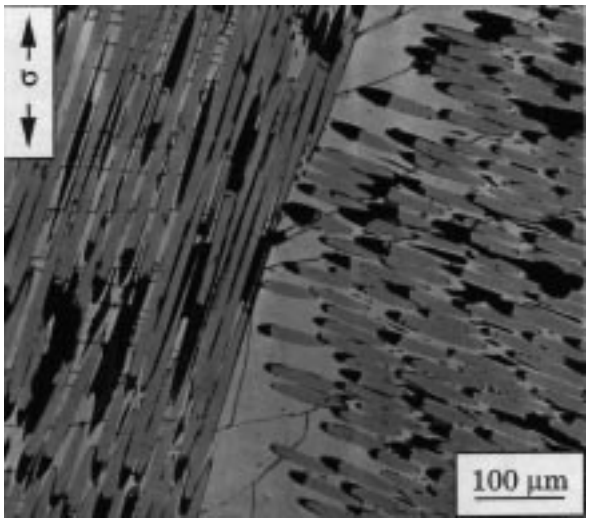

Fig. 5. Optical micrograph taken on a specimen tested to rupture in tension at 20° off-axis revealing both 45° shear induced matrix microcracks and microcracks normal to the fiber axis (plane (1,2)).

in the mathematical model through their equivalent effects on the elastic properties of the homogenized orthotropic continuum. As already stated, the hypothesis of a damageable-elastic behavior is justified by the weak residual strains and hysteretic effects observed from the interposed loading/unloading cycles. This means that the composite is considered as averagely free of residual stresses and that the non-linear dissipative effects are mainly attributed to damage.

Given these hypotheses, the constitutive law of the material may then be simply expressed in the initial orthotropy axes of the composite according to a generalized Hooke's law:

$$\varepsilon_i = \left(S^0_{ij} + \Delta S_{ij}\right)\sigma_j \quad (i,j = 1,2,6) \tag{2}$$

using the summation convention over repeated indices and the Voigt contracted notation where indices 1 and 2 represent the fiber directions while index 6 represents in-plane shear (with $\varepsilon_6 = 2\varepsilon_{12}$). ε_i and σ_i are the components of the strain tensor $\boldsymbol{\varepsilon}$ and the stress tensor $\boldsymbol{\sigma}$, respectively.

Damage variables used in CDM approaches are traditionally given non-dimensional values. The diagonal components of the internal damage variable $\Delta\mathbf{S}$ are thus normalized by their respective initial compliance values, which defines the three following scalar damage variables:

$$\omega_i = \frac{\Delta S_{ii}}{S^0_{ii}} \quad (i = 1,2,6). \tag{3}$$

3.1.2. Compressive behavior and damage deactivation

Eq. (2) applies to monotonic tensile and/or shear loadings for which damage is active, i.e. the microcracks are in the process of opening. In the case of complete crack closure, called passive damage or damage deactivation, the initial undamaged elastic properties are recovered. In order to take into account compressive loadings in the constitutive law, it is thus necessary to introduce an active/passive unilateral damage condition. For this purpose, an effective compliance tensor $\hat{\mathbf{S}}$ is considered, whose diagonal components are defined as follows (Chaboche et al., 1995):

$$\hat{S}_{ii} = S_{ii} + \big(1 - H(\hat{\sigma}_i)\big)\big(S^0_{ii} - S_{ii}\big) \quad (i = 1,2,6; \text{ no summation}), \tag{4}$$

where H represents the Heaviside function:

$$\begin{cases} H(x) = 0 & \text{if} \quad x < 0 \\ H(x) = 1 & \text{if} \quad x \geq 0 \end{cases},$$

and $\hat{\sigma}_{i=1,2,6}$ stands for equivalent deactivation stresses. In a first approximation, an active/passive condition based on a normal stress criterion may be retained in the case of tension/compression loadings performed within the fiber axes (Chaboche, 1993). However, for complex loadings containing both compressive and shear components, it is reasonable to state that complete crack closure will be linked to a 'competition' between these two stress components. As a consequence, the deactivation stress $\hat{\sigma}_6$ should be given a functional dependence towards the components of the stress tensor, hence:

$$\begin{cases} \hat{\sigma}_i = \sigma_i \quad i = 1,2 \\ \hat{\sigma}_6 = \hat{\sigma}_6(\sigma_1,\sigma_2,\sigma_6) \end{cases}. \tag{5}$$

The expression for $\hat{\sigma}_6$ will be explicitly established in a later section.

By combining Eqs. (3) and (4), the components of the effective compliance tensor finally become:

$$\hat{S}_{ii} = S^0_{ii}\big(1 + H(\hat{\sigma}_i)\omega_i\big) \quad (i = 1,2,6; \text{ no summation}). \tag{6}$$

3.1.3. Off-diagonal compliance tensor component

The off-diagonal component of the compliance tensor, S_{12}, is a coupling term whose changes may be viewed as an indirect consequence of damage, i.e. most probably linked to the extension of fiber/matrix debonding and/or to the opening of shear-induced 45° matrix cracks. Thus, the definition of a damage parameter ω_{12} related to the variation of S_{12} is mainly introduced in the present model for the sake of simplifying the notations, but will not be accompanied by an associated thermodynamic force (as defined in the next paragraph). Taking into account this consideration as well as, besides, the low values observed for the transverse strains, the following simple definition is thus retained:

$$\begin{cases} \omega_{12} = \dfrac{\Delta S_{12}}{\left|S^0_{12}\right|} \\ \hat{S}_{12} = S^0_{12}\big(1 - H(\hat{\sigma})\omega_{12}\big), \end{cases} \tag{7}$$

where $\hat{\sigma}$ is an equivalent deactivation stress aimed at restituting the initial value S^0_{12} upon compressive loadings, as attested experimentally from the 0° tension/compression test. The functional dependence of $\hat{\sigma}$ towards the components of the stress tensor will also be explicitly given in a later section.

The existence of a strain energy function imposes some thermodynamic restrictions on the variation of the damage parameters, as the compliance tensor should remain a positive defined operator all along the loading paths (Lemaître and Chaboche, 1985), hence:

$$S_{ii} > 0 \quad (i = 1,2,6; \text{ no summation}) \tag{8a}$$

$$S_{11}S_{22} - S^2_{12} > 0. \tag{8b}$$

Since damage is considered as a dissipative phenomenon and can thus only increase or remain stable, it follows that $\dot{\omega}_{i=1,2,6} \geq 0$, which is a sufficient (but unnecessary) condition for Eq. (8a) to be respected.

In the present case of the 2-D SiC/SiC composite, given the fact that S_{12} increases as damage takes place, and taking into account the initial tetragonal symmetry ($S_{11}^0 = S_{22}^0$), Eq. (8b) leads, with a little algebra, to the following thermodynamic restriction regarding ω_{12}:

$$\omega_{12} < 1 - \frac{S_{11}^0}{S_{12}^0}\sqrt{(1+\omega_1)(1+\omega_2)}. \tag{9}$$

3.2. Damage kinetics and constitutive law

Damage variables having been defined, constitutive equations describing the damage kinetics, i.e. the increase laws of these damage variables as a function of the imposed loading, are necessitated to complete the anisotropic damage model. A classical way to formulate both the constitutive law and the damage kinetics is to consider the framework of the thermodynamics of irreversible processes, in which two potentials are introduced (Bataille and Kestin, 1979; Germain et al., 1983):

- the thermodynamic potential, written as a function of the state variables, which defines the state (constitutive) laws and the conjugate variables associated to the state variables.
- the dissipation potential, written in the space of the associated variables, which accounts for the kinetics laws of evolution of the dissipative internal state variables.

3.2.1. Thermodynamic potential and constitutive laws

Since damage is considered as the only dissipative phenomenon responsible for the non linearities, the damage variables $\omega_{i\,=\,1,2,6}$ obviously constitute the dissipative internal state variables. The present definition of damage based on the change of the compliance tensor naturally dictates the choice of $\boldsymbol{\sigma}$ and T, respectively, the stress tensor and the absolute temperature, as the 'observable' state variables as well as of a thermodynamic potential based on the Gibbs free energy, Φ. For the present restriction to isothermal processes, it has been shown that the negative of the Gibbs free energy is merged with the complementary strain energy density function W^* (Fung, 1965), so that:

$$-\Phi = W^* = \frac{1}{2}\boldsymbol{\sigma}:\hat{\mathbf{S}}:\boldsymbol{\sigma}, \tag{10}$$

where the symbol (:) denotes the contracted product upon two indices.

By combining Eqs. (6), (7) and (10), it follows that the thermodynamic potential, now identified as W^*, may be expressed by:

$$\begin{aligned} 2W^* = {} & S_{11}^0\big(1 + H(\hat{\sigma}_1)\omega_1\big)\sigma_1^2 + S_{11}^0\big(1 + H(\hat{\sigma}_2)\omega_2\big)\sigma_2^2 + S_{66}^0\big(1 + H(\hat{\sigma}_6)\omega_6\big)\sigma_6^2 \\ & + 2S_{12}^0\big(1 - H(\hat{\sigma})\omega_{12}\big)\sigma_1\sigma_2. \end{aligned} \tag{11}$$

The conjugate variables associated with the state variables are then derived from the thermodynamic potential, as follows:

$$\boldsymbol{\varepsilon} = \left(\frac{\partial W^*}{\partial \sigma}\right)_{\omega} = \hat{\mathbf{S}}:\boldsymbol{\sigma} \tag{12a}$$

$$Y_i = \left(\frac{\partial W^*}{\partial \omega_i}\right)_{\sigma_i} = \frac{S_{ii}^0 H(\hat{\sigma}_i)\sigma_i^2}{2} \quad (i = 1,2,6). \tag{12b}$$

The variables Y_i are the thermodynamic forces associated with the damage variables ω_i, they represent the driving forces accounting for the kinetic laws of evolution of the dissipative damage variables. Within the CDM framework, these variables have the precise meaning of energy, released per volume, due to the advancement of damage and are thus referred to as 'energy density release rates' (Lemaître, 1992). As previously stated, the change of the off-diagonal compliance tensor component S_{12} being an indirect consequence of damage, the variable ω_{12} should not be viewed as a dissipative state variable and, consequently, does not define an associated thermodynamic force.

Eq. (12a) establishes the constitutive (state) law of the material which, by deriving from the state potential, thus ensures a continuous relationship between stresses and strains:

$$\begin{cases} \varepsilon_1 = S_{11}^0\big(1 + H(\hat{\sigma}_1)\omega_1\big)\sigma_1 + S_{12}^0\big(1 - H(\hat{\sigma})\omega_{12}\big)\sigma_2, \\ \varepsilon_2 = S_{12}^0\big(1 - H(\hat{\sigma})\omega_{12}\big)\sigma_1 + S_{11}^0\big(1 + H(\hat{\sigma}_2)\omega_2\big)\sigma_2 \\ \varepsilon_6 = S_{66}^0\big(1 + H(\hat{\sigma}_6)\omega_6\big)\sigma_6. \end{cases} \tag{13}$$

In order to be thermodynamically consistent, the Clausius–Duhem inequality, which contains both the first and the second principle of thermodynamics and accounts for a positive dissipation, has to be verified. In the present case of damage growth being assumed as the only dissipative phenomenon and for an isothermal process, this inequality reduces to:

$$Y_i\dot{\omega}_i \geq 0 \quad i = 1,2,6. \tag{14}$$

Considering that the thermodynamic forces Y_i are always positive and that the above inequality should hold for any given loading, this principle will then be automatically checked if (and only if) the complementary laws describing the damage kinetics respect the conditions $\dot{\omega}_{i=1,2,6} \geq 0$.

3.2.2. Dissipation potential and damage kinetics

The requirement of positive internal dissipation gives the motivation to postulate the existence of a dissipation potential, written in the generalized space of the associated thermodynamic forces, from which are derived the damage kinetic laws. In the present case, within the simplifying assumption of a time independent process, an associated framework is used in which the dissipation potential is replaced by damage criterion functions describing the surface limiting the undamaged domain (Ladevèze, 1994; Chaboche et al., 1995).

The difference observed in the damage modes induced by tensile and shear loadings suggests the choice of coupled multiple criteria, one for each damage variable. Considering, besides, the initial tetragonal symmetry of the material which imposes an equivalence of this multicriteria in directions 1 and 2, the evolution of the damage variables is given the following general form:

$$\begin{cases} \omega_1 = f_1\big(\langle Y_1^* - Y_{01}\rangle\big), \\ \omega_2 = f_1\big(\langle \underline{Y_2^*} - Y_{01}\rangle\big) \\ \omega_6 = f_6\big(\langle \underline{Y_6^*} - Y_{06}\rangle\big), \end{cases} \tag{15a}$$

with the notation:

$$\underline{x(t)} = \operatorname*{Sup}_{\tau \leq t}(x(\tau)). \tag{15b}$$

The symbol $\langle . \rangle$ signifies the McAuley bracket with its usual definition: $\langle x \rangle = 1/2(x + |x|)$, f_1 and f_6

represent the principal damage threshold functions for tensile and shear loadings, respectively, whereas Y_{01} and Y_{06} stand for the initial damage thresholds. The use of the McAuley bracket thus simply states that no damage occurs as long as these initial thresholds are not exceeded (providing functions f_1 and f_6 are taken to be zero at the origin).

$Y^*_{i=1,2,6}$ are scalar functions of the thermodynamic forces $Y_{i\,=\,1,2,6}$ representing the equations of the damage surfaces. The supremum taken over the Y^*_i is aimed at storing the loading history by stating that the values at a given time t of the damage variables will increase only if the maximum value of Y^*_i reached during previous loadings is exceeded. Positive dissipation, together with the assumption that the damage kinetic laws are derived from a multisurface potential, require the scalar functions f_1 and f_6 to be positive and monotonously increasing, and the damage surfaces $Y^*_{i=1,2,6}$ to be positive and at least star convex with respect to the origin (Matzenmiller et al., 1995).

The equations of the damage surfaces are explicitly expressed as:and

$$\begin{cases} Y^*_1 = \left[\left(Y^n_1 + (g_{12}(\underline{Y_2})Y_2)^n \right)^{m/n} + (g_{16}(\underline{Y_6})Y_6)^m \right]^{1/m}, \\ Y^*_2 = \left[\left(Y^n_2 + (g_{12}(\underline{Y_1})Y_1)^n \right)^{m/n} + (g_{16}(\underline{Y_6})Y_6)^m \right]^{1/m} \\ Y^*_6 = \left[Y^m_6 + ((g_{61}(\underline{Y_1})Y_1)^n + (g_{61}(\underline{Y_2})Y_2)^n)^{m/n} \right]^{1/m}. \end{cases} \tag{16}$$

The exponents m and n are positive constant coefficients aimed at adjusting the coupling intensity between the thermodynamic forces while avoiding the introduction of quadratic terms (always difficult to identify experimentally).

g_{12}, g_{16} and g_{61} are non-dimensional positive scalar functions accommodating the coupling of growth for the individual damage variables in the various damage modes. These coupling terms are not *a-priori* described by constant coefficients for the microstructural observations revealed, whatever the imposed loading, matrix microcracks and induced debonds of different characteristic sizes and surrounding media taking place sequentially. Each of these damage entities should thus be expected to influence differently the variation of the compliance tensor components.

Given the restrictions previously established, the evolution law of ω_{12} is simply assumed to be directly linked to the damage variables $\omega_{i\,=\,1,2,6}$:

$$\omega_{12} = f(\omega_1, \omega_2), \tag{17}$$

where f is a material-dependent non-dimensional function. Such a formulation implies that shear components only indirectly influence S_{12} through their coupling effects in ω_1 and ω_2. In order to maintain consistency with both the observed mechanical behavior in tension/compression within the fiber axes and the thermodynamic restriction given by Eq. (9), Eq. (17) is further explicited as:

$$\omega_{12} = \begin{cases} \min(f(\underline{\omega^*}), 1) & \text{if} \quad \underline{H_0(\dot{\omega}_6)Y_6} = 0 \\ \min\left(f(\underline{\omega^*}), \omega^{\max}_{12}\right) & \text{if} \quad \underline{H_0(\dot{\omega}_6)Y_6} > 0 \end{cases} \tag{18a}$$

with

$$\begin{cases} \underline{\omega^*} = \underset{\tau \le t}{\text{Sup}}[H_0(\sigma_1)\omega_1 + H_0(\sigma_2)\omega_2]_{|\tau} \\ \omega^{\max}_{12} = 1 - \dfrac{S^0_{11}}{S^0_{12}}\sqrt{(1+\omega_1)(1+\omega_2)}, \end{cases} \tag{18b}$$

where function H_0, introduced for the sake of simplifying the notations, only differs from the usual Heaviside function by its definition at the origin: $H_0(0)=0$.

The positiveness of the expression $\underline{H_0(\dot{\omega}_6)Y_6}$ serves as a condition indicating the presence of shear induced 45°-microcracks: Shear damage is supposed to take place if an increase of the shear damage parameter ω_6 occurs in conjunction with the presence of a shear stress component in the imposed loading.

3.2.3. Active/passive damage evolution

As previously indicated, the complete closure of the microcracks present in the material generates a passive damage state for which the initial elastic properties are recovered. In this respect, the following two main problems related to the presence of a shear component in the imposed loading have to be addressed:

(i) shear load reversal: if the shear stresses are reversed, the principal stresses interchange their directions. Since the shear-induced microcraks are inclined at 45° to the fiber axis, a shear load reversal will thus tend to close one system of cracks (e.g. at $+45°$) while activating the opposite system (at $-45°$)
(ii) compression/shear loadings: the superposition of a compression state over a shear component should either impede shear damage or at least slow down the shear damage kinetics if the shear component takes over.

3.2.3.1. Shear load reversal. The two sets of microcracks induced by shear stresses of opposite sign lead to consider two distinct damage variables ω_6^+ and ω_6^- with their associated equivalent deactivation stresses $\hat{\sigma}_6^+$ and $\hat{\sigma}_6^-$ defined by:

$$H(\hat{\sigma}_6)\omega_6 = H\big(\hat{\sigma}_6^+\big)\omega_6^+ + H\big(\hat{\sigma}_6^-\big)\omega_6^-. \tag{19}$$

Bringing Eq. (19) into the expression of the thermodynamic potential and making use of Eqs. (12a) and (12b) yields:

$$\varepsilon_6 = S_{66}^0\Big(1 + H\big(\hat{\sigma}_6^+\big)\omega_6^+ + H\big(\hat{\sigma}_6^-\big)\omega_6^-\Big)\sigma_6, \tag{20}$$

and

$$\begin{cases} Y_6^+ = \dfrac{S_{66}^0 H\big(\hat{\sigma}_6^+\big)\sigma_6^2}{2} \\ Y_6^- = \dfrac{S_{66}^0 H\big(\hat{\sigma}_6^-\big)\sigma_6^2}{2}. \end{cases} \tag{21}$$

Eq. (20) thus formally replaces the shear component in the constitutive law (Eq. (14)) whereas the thermodynamic forces Y_6^+ and Y_6^- allow us to establish the kinetic laws of evolution of the damage variables, ω_6^+ and ω_6^-, defined as follows:

$$\begin{cases} \omega_6^+ = f_6\Big(\underset{\tau\le t}{\mathrm{Sup}}\langle \underline{Y_6^{*+}} - A\big(Y_6^-\big)Y_{06}\rangle_{|\tau}\Big) \\ \omega_6^- = f_6\Big(\underset{\tau\le t}{\mathrm{Sup}}\langle \underline{Y_6^{*-}} - A\big(Y_6^+\big)Y_{06}\rangle_{|\tau}\Big), \end{cases} \tag{22a}$$

with

$$\begin{cases} Y_6^{*\pm} = \left[\left(Y_6^{\pm} \right)^m + \left(\left(g_{61}(\underline{Y_1}) Y_1 \right)^n \right) + \left(g_{61}(\underline{Y_2}) Y_2 \right)^n \right)^{m/n} \right]^{1/m} \\ A\left(Y_6^{\pm} \right) = 1 + \alpha \dfrac{H_0(\dot{\omega}_6) Y_6^{\pm}}{Y_{06}}, \end{cases} \tag{22b}$$

where A is a non-dimensional scalar function accounting for a possible dependence of the damage kinetics: even deactivated, cracks are still present which may thus lead to an increase of the damage threshold upon shear reversal. Since microcracks of the same type are concerned, it has been *a-priori* postulated that this dependence may be described by a positive constant coefficient, α.

Conversely, the thermodynamic force Y_6 interacting in the kinetic laws of evolution of the damage variables ω_1 and ω_2 (Eqs. (15a), (15b) and (16)) is, in a first approximation, simply defined by:

$$Y_6 = Y_6^+ + Y_6^-. \tag{23}$$

3.2.3.2. Compression/shear loadings. Following Poss and Ladevèze (Poss, 1982; Ladevèze, 1994), it is assumed that the global compression state represents the driving force accounting for the partial/total impediment of the shear damage kinetics. A new force, Z, based on the hydrostatic compression stress is thus defined:

$$Z = \langle -(\sigma_1 + \sigma_2) \rangle. \tag{24}$$

The thermodynamic forces Y_6^+ and Y_6^- associated with the shear damage variables, ω_6^+ and ω_6^-, are then formally replaced in the equations describing the damage kinetics (i.e. Eqs. (16), (22a), (22b) and (23)) by two functions of Z, $B(Y_6^+, Z)$ and $B(Y_6^-, Z)$, respectively. A possible choice for function B, allowing a good description of the impediment effect with a limited number of parameters, is given by:

$$B\left(Y_6^{\pm} \right) = \langle Y_6^{\pm} - \beta Z^2 \rangle, \tag{25}$$

where β is a positive constant having the dimension of a compliance.

The evaluation of the shear equivalent deactivation stresses $\hat{\sigma}_6^+$ and $\hat{\sigma}_6^-$ is now straightforward when assuming that a common criterion should define both the shear/compression 'competition' in the damage kinetics and the deactivation condition (i.e. function B written in this later case in terms of stresses). More precisely, such an assumption signifies that for a loading state located inside the loading surface, shear cracks are considered as deactivated if the condition for a possible further shear damage is not satisfied ($B = 0$) and activated in the opposite case ($B > 0$). A rearrangement of Eq. (25) thus directly yields:

$$\begin{cases} \hat{\sigma}_6^+ \propto \sigma_6 - \left(\dfrac{2\beta Z^2}{S_{66}^0 |\sigma_6|} \right) \\ \hat{\sigma}_6^- \propto -\sigma_6 - \left(\dfrac{2\beta Z^2}{S_{66}^0 |\sigma_6|} \right) \end{cases} \quad \text{if } \sigma_6 \neq 0$$

and

$$\hat{\sigma}_6^{\pm} \propto -Z^2 \quad \text{if } \sigma_6 = 0. \tag{26}$$

Similarly, it is also assumed that the total recovery of the initial off-axis compliance component (Eq. (7)) is directly linked to an hydrostatic compression state, hence:

$$\hat{\sigma} = -Z. \tag{27}$$

3.3. Failure prediction

The present purpose is not to establish a true rupture theory transposable at the level of real structures but to give a good description of the ultimate damage state before the critical conditions, i.e. slightly before the onset of a macrocrack leading to final rupture. A multicriterion depending from the type of loading and relating the different rupture criteria to different rupture mechanisms has been adopted.

3.3.1. Tensile loadings

Under pure tension, final failure of the composite appears to result from a brittle fracture of the fiber bundles and is therefore represented by a critical stress. However, in order to take into account the damage induced progressive stress redistribution to the fibers (i.e. the usual composite effect), this critical stress is expressed in terms of an effective stress instead of the nominal stress. The effective stress tensor ($\tilde{\boldsymbol{\sigma}}$) is related to the damage variables in the classical sense of CDM through a simple relationship (Lemaître, 1992; Ladevèze, 1994):

$$\mathbf{S}_0 : \tilde{\boldsymbol{\sigma}} = \hat{\mathbf{S}} : \boldsymbol{\sigma} \Longrightarrow \tilde{\boldsymbol{\sigma}} = \left(\mathbf{S}_0^{-1} : \hat{\mathbf{S}}\right) : \boldsymbol{\sigma} \tag{28}$$

which yields:

$$\tilde{\sigma}_i = (1 + H(\hat{\sigma}_i)\omega_i)\sigma_i \quad i = 1,2,6. \tag{29}$$

Fracture takes place when $\tilde{\sigma}_i = \tilde{\sigma}_i^r$ ($i = 1,2$), $\tilde{\sigma}_i^r$ being identified by mean of a simple tensile test performed within the fiber axis.

3.3.2. Shear loadings

As may be observed from the stress/strain curve derived from the Iosipescu shear test (Fig. 3), shear rupture roughly corresponds to an instability condition (i.e. $\dot{\sigma}_6 = 0$ with $\dot{\varepsilon}_6 \neq 0$). This is in line with the fact that, under pure shear, the matrix is more prompted than the fibers. Consequently, the influence of a shear component on the rupture behavior is introduced through a critical shear damage value, ω_6^r, obtained from the Iosipescu shear test at the instability (peak) point.

3.3.3. Compressive loadings

Results obtained from the compression tests suggest that, contrary to tensile loadings, all the compressive components play a part in the rupture behavior. Following a suggestion made in reference (Ladevèze et al., 1994), a rupture criterion based on a maximum compression energy is therefore retained. The compression energy, W_c^*, is derived from the expression of the thermodynamic potential (Eq. (11)) by introducing the classical decomposition:

$$\sigma_i = \langle \sigma_i \rangle - \langle -\sigma_i \rangle \; i = 1,2. \tag{30a}$$

Making use of the expressions of the equivalent deactivation stresses (i.e. $\hat{\sigma}_i = \sigma_{i=1,2}$, [Eq. (5)]) and of

the following properties:

$$\begin{cases} x^2 = \langle x \rangle^2 + \langle -x \rangle^2 \\ \langle x \rangle \langle -x \rangle = 0, \end{cases} \tag{30b}$$

one finally obtains:

$$W_c^* = \frac{S_{11}^0}{2}\left(\langle -\sigma_1 \rangle^2 + \langle -\sigma_2 \rangle^2\right). \tag{31}$$

Fracture is supposed to occur when W_c^* reaches a critical value, denoted E_c, which may be determined experimentally by a simple on-axis compression test.

Finally, under complex multiaxial loadings, it is assumed that rupture intervenes as soon as one of the failure criteria described above is reached, hence:

$$\begin{cases} r_i = \dfrac{\tilde{\sigma}_i}{\tilde{\sigma}_i^r} - 1 \quad i = 1,2, \\ r_6 = \dfrac{\omega_6}{\omega_6^r} - 1 \\ r_0 = \dfrac{W_c^*}{E_c} - 1; \end{cases} \tag{32a}$$

$$F = \mathrm{Sup}_i(r_i) \begin{cases} \geq 0 & \text{failed} \\ < 0 & \text{unfailed} \end{cases}. \tag{32b}$$

4. Application to the 2-D SiC/SiC material

4.1. Model identification

The identification of the functions and parameters describing the model is performed with the help of the experimental results displayed in Section 2.

The first step is to identify the initial compliance coefficients (S_{11}^0, S_{66}^0 and S_{12}^0), the initial damage thresholds (Y_{01} and Y_{06}) and the principal damage threshold functions (f_1 and f_6). This is done by considering the stress–strain response of both the on-axis tensile test and the Iosipescu shear test, and by plotting the respective evolution of the damage variables, ω_1 and ω_6, as a function of their thermodynamic forces, Y_1 and Y_6 (Fig. 6). Appropriate forms of evolution law fitting the data shown in Fig. 6 have been established as:

$$f_1 \rightarrow \omega_1 = \left(\frac{\langle Y_1^* - Y_{01} \rangle}{Y_{1c}} \right)^{a_1}, \tag{33}$$

where Y_{1c} is a normalizing force and a_1 is a shape exponent.

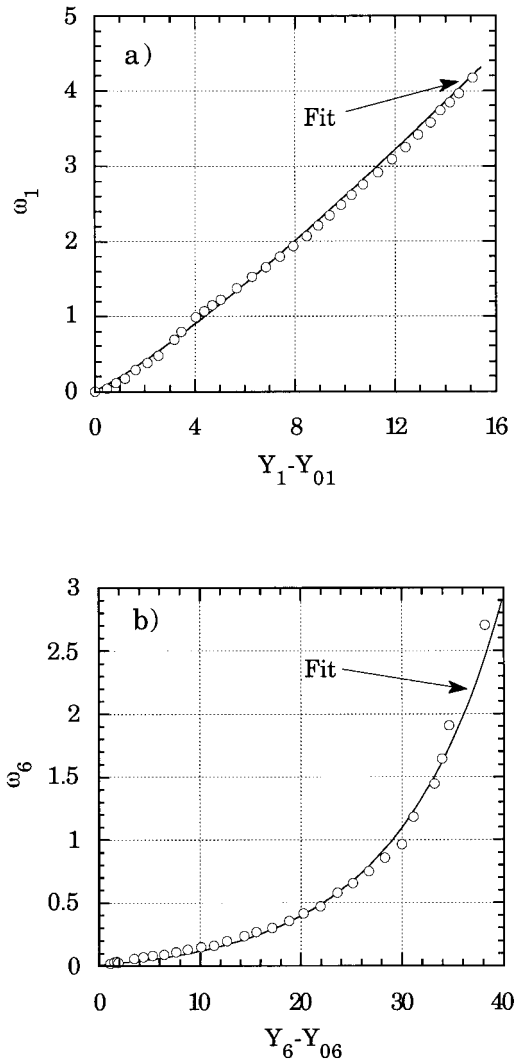

Fig. 6. Experimental and fitted identification of the damage threshold functions f_1 (a) and f_6 (b).

$$f_6 \rightarrow \omega_6 = \left(Ln\left(1 - \frac{\langle Y_6^* - Y_{06} \rangle}{Y_{6\infty}} \right)^{-a_6} \right)^{b_6}, \tag{34}$$

where $Y_{6\infty}$ is a saturation force and a_6, b_6 are positive shape exponents.

The transverse strain response of the on-axis tensile test allows to plot the variation of the off-diagonal component S_{12} as a function of ω_1, which leads to the identification of function f. This function has been fairly fitted by a simple linear law:

$$\omega_{12} \rightarrow f(\underline{\omega^*}) = 0.34\underline{\omega^*}. \tag{35}$$

These two tests, with the addition of the on-axis compression test, give easy access to the three

constants defining the rupture criterion, identified as:

$$\tilde{\sigma}_1^r = 1.51 \text{ GPa},$$

$$\omega_6^r = 4.85$$

$$E_c = 450 \text{ kJ/m}^3. \tag{36}$$

The initial assumption of preserved orthotropy all along the loading path allows to consider off-axis

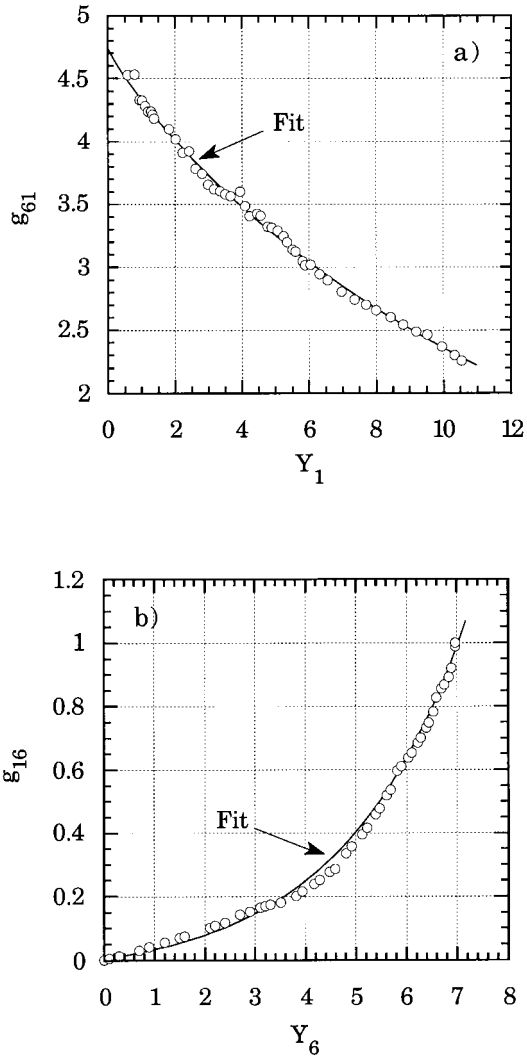

Fig. 7. Experimental and fitted identification of the coupling functions g_{61} (a) and g_{16} (b).

tests as being representative of multiaxial proportional loadings. The identification of the equations of the damage surfaces, i.e. functions g_{ij} and exponents m and n, may thus be simply achieved by using the two previously determined functions, f_1 and f_6, and the stress–strain responses of the 20° and 45° off-axis tensile tests (as projected in the orthotropy axes). A simple numerical optimization method is used to adjust m and n so that function g_{61} obtained from the stress–strain response $\varepsilon_6-\sigma_6$ of the 20° and 45° off-axis tests coincides at the best. A similar procedure is used with the three independent strain responses ε_1 (20°), ε_2 (20°), ε_1 (45°) (i.e. at 45° off-axis, given the balance symmetry, $\varepsilon_1=\varepsilon_2$) to determine functions g_{12} and g_{16}. Examples of graphs of some of the coupling functions thus obtained are given in Fig. 7. Appropriate forms of the evolution laws fitting these functions have been established as follows:

$$g_{12}(Y_2) = A_{12}\exp\left(-\left(\frac{\langle Y_2 - Y_S\rangle}{Y^{c}_{12}}\right)^{a_{12}}\right) + B_{12}, \tag{37}$$

$$g_{16}(Y_6) = A_{16}\left(\exp\left(\left(\frac{Y_6}{Y^{c}_{16}}\right)^{a_{16}}\right) - 1\right) \tag{38}$$

$$g_{61}(Y_1) = A_{61}\exp\left(-\left(\frac{Y_1}{Y^{c}_{61}}\right)^{a_{61}}\right) + B_{61}. \tag{39}$$

Optimized values of the coupling exponents m and n have been identified as:

$$m = 0.5;\ n = 1.1. \tag{40}$$

The final step consists in setting up the values of the two constants α and β which govern the damage kinetics upon reverse shear and compression/shear loadings, respectively. In the absence of appropriate experimental guidance, a rough estimation of α was derived from the results of a reversed Iosipescu shear test performed on a closely related material [CVI-processed 2-D C/SiC (Camus and Baste, 1998)]. Similarly, constant β could not be identified from the set of experiments reported in Section 2, since no damage was evidenced upon off-axis compression tests. A realistic value for constant β was thus derived from a torsion/compression test performed at ONERA (with a ratio $\tau/\sigma=-1$) on a tube made of a similar CVI-processed 2-D woven SiC/SiC composite (Maire and Pacou, 1996). The values retained for these two constants are:

$$\alpha = 0.15;\ \beta = 0.0025\ \mathrm{GPa}^{-1}. \tag{41}$$

4.2. Experimental verification and discussion

Once the identification procedure has been completed, the constitutive law is then computed in view of performing numerical simulations of the mechanical response of the composite subject to complex loading conditions. It should be emphasized that the explicit character of the model renders the computational flow chart very simple since no iterative algorithm is locally required at each loading step.

Fig. 8 displays a comparison between the experiments and the computations of various on-axis and off-axis tension and compression tests. The excellent agreement observed between the model and the experiments in terms of stress–strain curves as well as of ultimate failure confirms the pertinence of the basic assumptions made to build up the model and supports the validity of the failure criterion.

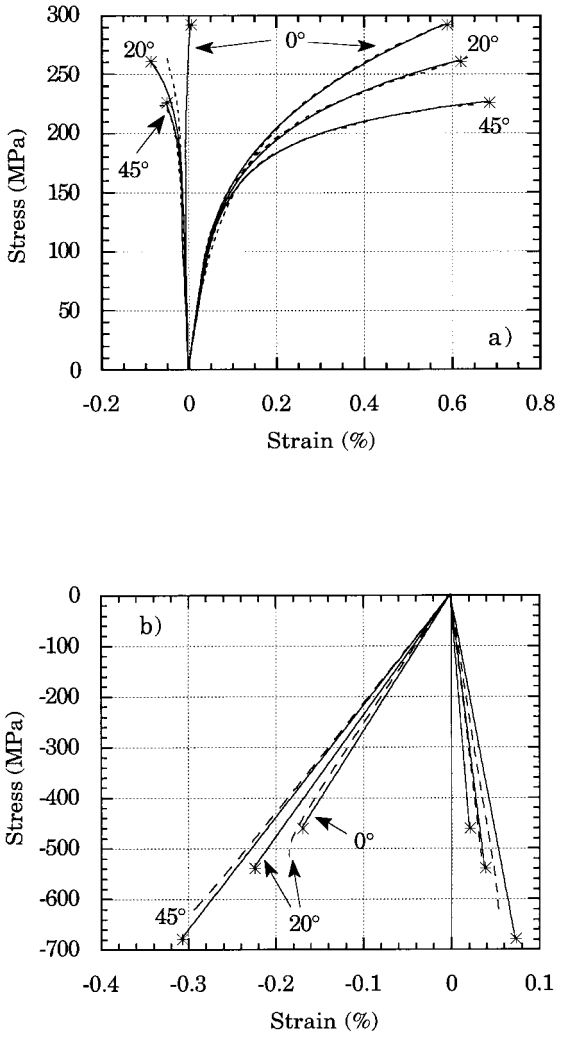

Fig. 8. Comparisons between simulations (solid lines) and experimental data (dotted lines) for tension tests (a) and compression tests (b) performed at 0°, 20° and 45°. Stars indicate the calculated failures.

Fig. 9 shows a comparison between the experimental and the simulated stress–strain behavior of the material submitted to a 45° off-axis tension/compression test, which evidences a correct description of damage deactivation when unloading cycles are prolonged in the compression domain.

In order to increase the validity domain, it is necessary to measure the ability of the constitutive law to predict the mechanical behavior of the material when the stress state is different from those used in the identification procedure. To this end, numerical simulations of biaxial tests formally performed by Aubard on 2-D SiC/SiC 0.4% thin wall tubes (Aubard, 1992, 1995) have been made.

Fig. 10 shows the experimental results and the numerical predictions of an internal pressure test (interrupted before rupture) corresponding to an imposed biaxial stress state with $\sigma_2 = 2\sigma_1$. A good agreement may be observed between experimental data and predictions, more specifically regarding the

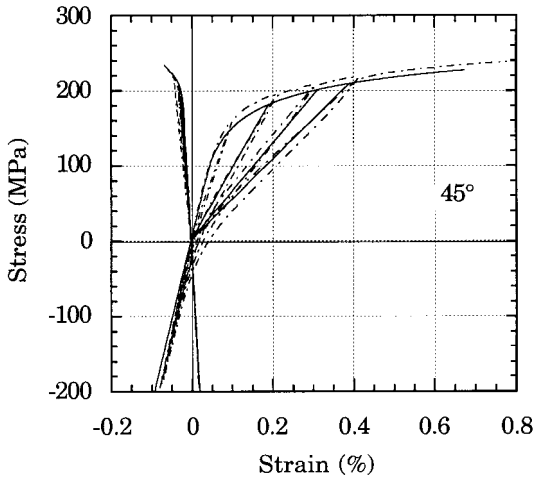

Fig. 9. Comparison between simulation (solid line) and experimental data (dotted line) for a 45° off-axis tension/compression test.

restitution of the differences between the axial behavior and the circumferential behavior which account for the damage-coupling effect between the two principal orthotropy axes.

Experimental and predicted shear stress–strain curves derived from a torsion test (experimentally interrupted before rupture at 135 MPa) performed on the tube initially damaged under internal pressure loading are plotted in Fig. 11. Comparison made with a torsion test performed on a virgin specimen reveals a good ability of the model in restituting, at least qualitatively, the observed damage-coupling effect of the initial biaxial tensile loading on the subsequent shear behavior. However, some discrepancy takes place when considering both the initial shear modulus and the shear damage threshold for which the model predicts a value over 135 MPa. Given the specific non-proportional/sequential multiaxial state of loading retranscribed by this test, this discrepancy should most likely be related to the initial assumption of damageable-elasticity which led to neglect frictional sliding and the resulting hysteretic

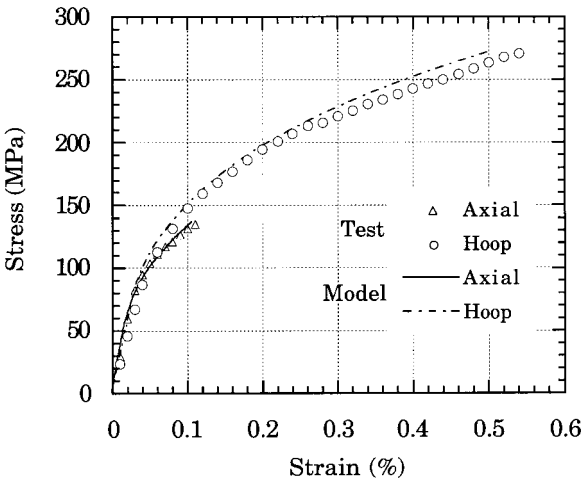

Fig. 10. Comparisons between simulation and experimental data (after Aubard, 1992) for an internal pressure tube test (interrupted before rupture).

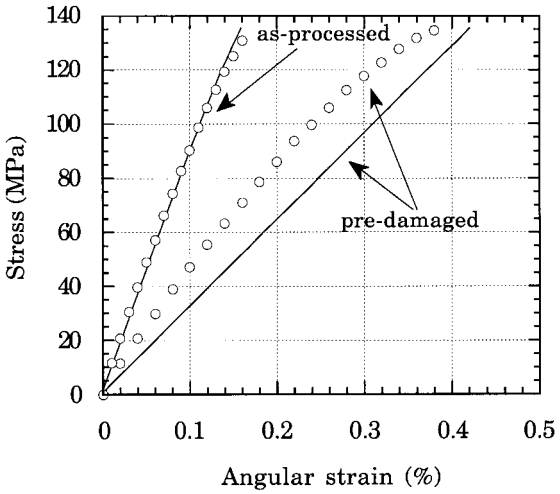

Fig. 11. Experimental (circles, after Aubard, 1992) and simulated (solid lines) shear stress/strain curves derived from torsion tests performed on a virgin specimen and on the tube initially damaged under internal pressure loading (tests interrupted before rupture at 135 MPa).

crack opening displacements taking place in the course of unloading/reloading cycles. As a matter of fact, crack-reopening with frictional sliding is largely responsible for the initial non-linearity observed upon the reloading part of the cycles. Such an effect will obviously be intensified when a shear component, which corresponds to a 45° tension/compression biaxial loading, is added to pre-existing tensile cracks (i.e. normal and/or parallel to the fiber axis). This tentative explanation is supported by post-mortem morphological observations which have confirmed that no new cracks were generated in torsion up to the maximum applied stress of 135 MPa, i.e. the non-linear behavior displayed experimentally may be mostly attributed to frictional sliding.

5. Conclusions

A macroscopic model for the non-linear analysis of orthotropic CMCs submitted to complex multiaxial loadings has been presented within the framework of Continuum Damage Mechanics. The complicated process of damage development is reduced to the use of four state variables, the total imposed stress and three phenomenological internal damage variables. The kinetic laws accounting for the growth of the internal variables are given by coupled multiple damage criteria written in the generalized space of associated thermodynamic forces and defined with the help of microstructural observations of the dominating physical phenomena.

Application of the present model to a 2-D woven SiC/SiC composite requires the identification of a reduced set of material dependent functions and parameters, namely: (i) two principal damage threshold functions, four coupling functions and two constants associated to shear damage evolution, all accounting for damage kinetics and (ii) three constants describing final failure. Moreover, it is shown that most of these functions and parameters (at the exception of the constant describing compression/shear interactions) may be easily identified from few simple uniaxial tests.

Comparisons between experiments and numerical simulations reveal a good ability of the model for describing the non-linear behavior observed under various on-axis and off-axis uniaxial loading

conditions. The good agreement seen with the simulation of an internal pressure tube test represents a promising result for the prediction of real multi-axial loadings, at least when performed under proportional conditions. The damage deactivation effects taking place in compression as well as the rupture behavior are also accurately described. An important issue yet remaining to be addressed is the incorporation of the hysteretic effects linked to frictional sliding which seem to be no longer negligible under certain non-proportional loading states.

This model is well suited for an easy implementation in standard finite element codes and may thus be used to predict the damage state of a structure during the initiation stage, i.e. before damage localization. It is also possible to extend the present approach to other CMCs, providing that the processing related residual stress field generally observed may be taken into account.

Acknowledgements

The author would like to thank B. Humez (LCTS) for performing the mechanical tests as well as J. Pailhès (LCTS) and X. Aubard (SEP) for helpful comments and discussions.

References

Aubard, X., 1992. Mechanical behaviour models of 2-D SiC–SiC composites. Ph.D. thesis, University of Paris 6, France.

Aubard, X., 1995. Modelling of the mechanical behaviour of a 2-D SiC–SiC composite at a meso-scale. Comp. Sci. Technol. 54, 371–378.

Aussedat, E., Thionnet, A., Renard, J., 1993. Modelling of damage in composite materials submitted to off-axis loadings. Application to woven SiC/SiC. Revue Comp. Mat. Avancés 3 (2), 181–193 (in French).

Baste, S., Audouin, B., 1991. On internal variables in anisotropic damage. Eur. J. of Mech. A Solids 10 (6), 587–606.

Bataille, J., Kestin, J., 1979. Irreversible processes and physical interpretations of rational thermodynamics. J. Non Equil. Thermodyn. 4, 229–258.

Burr, A., Hild, F., Leckie, F.A., 1995. Micro-mechanics and continuum damage mechanics. Arch. Appl. Mech. 65 (7), 437–456.

Burr, A., Hild, F., Leckie, F.A., 1997. Continuum description of damage in ceramic-matrix composites. Eur. J. Mech. A/Solids 16 (1), 53–78.

Cady, C., Heredia, F.F., Evans, A.G., 1995. In-plane mechanical properties of several ceramic matrix composites. J. Am. Ceram. Soc. 78 (8), 2065–2078.

Camus, G., Baste, S., 1998. Development of damage in a 2-D woven C/SiC composite under off-axis and shear loadings. Internal Report, L.C.T.S.

Chaboche, J.L., 1993. Development of continuum damage mechanics for elastic solids sustaining anisotropic and unilateral damage. Int. J. of Damage Mech. 2, 311–329.

Chaboche, J.L., Lesne, P.M., Maire, J.F., 1995. Macroscopic modelling and damage processes in CMCs. Ceram. Trans. 57, 65–75.

Cluzel, C., Allix, O., Ladevèze, P., Peres, P., 1992. Damage meso-modelling of 3-D evolutive composite. In: Bunsell, A.R., Jamet, J.F., Massiah, A. (Eds.), Developments in the Science and Technology of Composite Materials, ECCM5. European Association for Composite Materials, Bordeaux, pp. 591–596.

Duvaut, G., 1976. Functional analysis and continuum mechanics. Application to the study of elastic composite materials with periodic structures. In: Koiter, W.T. (Ed.), Theoretical and Applied Mechanics. North–Holland, pp. 119–132 (in French).

Evans, A.G., Marshall, D.B., 1989. The mechanical behavior of ceramic matrix composites. Acta. Metall. 37, 2567–2583.

Fung, Y.C., 1965. Foundations of Solid Mechanics. Prentice–Hall Inc, Englewood Cliffs, New Jersey.

Germain, P., Nguyen, Q.S., Suquet, P., 1983. Continuum thermodynamics. J. Appl. Mech. 50, 1010–1020.

Gudmundson, P., Ostlund, S., 1992. Prediction of thermoelastic properties of composite laminates with matrix cracks. Comp. Sci. Technol. 44, 95–105.

Guillaumat, L., 1994. Microcracking of CMCs: Relationships with the microtexture and the mechanical behavior. Ph.D. thesis, University of Bordeaux, France.

Harris, C.E., Lee, J.W., Allen, D.H., 1989. Internal state variable approach for predicting stiffness reduction in fibrous laminated composites with matrix cracks. J. Comp. Mat. 23, 1273–1291.

Jouin, J.M., Cotteret, J., Christin, F., 1993. SiC/SiC interphase: case history. In: Peteves, S.D. (Ed.), Designing Ceramic Interfaces II. Commission of the European Communities, Brussels, Luxembourg, pp. 191–203.

Kachanov, L.M., 1958. Time of the rupture process under creep conditions. Izv. Akad. Nauk., S.R.S., Odt. Tekh. Nauk 8, 26–31.

Krajcinovic, D., 1989. Damage mechanics. Mech. Mat. 8, 117–197.

Ladevèze, P., 1994. Inelastic strains and damage. In: Talreja, R. (Ed.), Damage Mechanics of Composite Materials. Elsevier Science B.V, pp. 117–138.

Ladevèze, P., Gasser, A., Allix, O., 1994. Damage mechanisms modeling for ceramic composites. J. Eng. Mat. Tech. 116, 331–336.

Laws, N., Dvorak, G.J., 1987. The effect of fiber breaks and aligned penny-shaped cracks on the stiffness and energy release rates in unidirectional composites. Int. J. Solids Struct. 23, 1269–1283.

Lemaître, J., Chaboche, J.L., 1985. Mechanics of Solid Materials. Bordas, Paris (in French).

Lemaître, J., 1992. A Course on Damage Mechanics. Springer–Verlag, Berlin, Heidelberg.

Maire, J.F., Pacou, D., 1996. Tension–compression–torsion tests on ceramic-matrix composite tubes. In: Baptiste, D., Vautrin, A. (Eds.), JNC 10, vol. 3. AMAC, Paris, France, pp. 1225–1234 (in French).

Matzenmiller, A., Lubliner, J., Taylor, R.L., 1995. A constitutive model for anisotropic damage in fiber-composites. Mech. Mat. 20, 125–152.

Ortiz, M., 1985. A constitutive theory for the inelastic behavior of concrete. Mech. Mat. 4, 67–93.

Poss, M., 1982. Damage and rupture of carbon–carbon composite materials. Ph.D. thesis, University of Paris VI, France.

Talreja, R., 1991. Continuum modelling of damage in ceramic matrix composites. Mech. Mat. 12, 165–180.

Wang, S.W., Parvizi-Majidi, A., 1992. Experimental characterization of the tensile behaviour of Nicalon fibre-reinforced calcium aluminosilicate composites. J. Mater. Sci. 27, 5483–5496.